Preparation of undoped and Zn-doped TiO_2 by sol-gel method with two different procedures and photocatalytic degradation on phenol

JI-GUO HUANG[a], SHUO PANG[a], BO WANG[a], HONG-YU MA[a], MENG-YANG ZHENG[a], LI-LI DONG[b,c,*], XING-JUAN LIU[a]

[a]*Key Laboratory of Groundwater Resources and Environment, Ministry of Education, Jilin University, Changchun 130026, PR China*

[b]*Key Laboratory of Songliao Aquatic Environment, Ministry of Education, Jilin Jianzhu University, Changchun 130118, PR China*

[c]*School of Environment, Northeast Normal University, Changchun 130117, PR China*

The undoped and Zn-doped TiO_2 nanoparticles were synthesized by sol-gel method with two different procedures. The photocatalytic activity was evaluated by photodegradation experiments of phenol. The effects of calcination temperatures and Zn doping amounts were discussed. It was found that the photocatalytic activity of TiO_2 prepared by procedure B is much higher than TiO_2 prepared by procedure A. When the calcination temperature was 450℃ and the Zn doping amount was 4%, the Zn-doped TiO_2 sample exhibited the highest photocatalytic activity. Zn doping was shown to be an efficient method for phenol degradation under visible light, especially under solar light.

(Received October 20, 2014; accepted January 21, 2015)

Keywords: Zn-doped TiO_2, Sol-gel method with two different procedures, Phenol degradation, Solar light

1. Introduction

In recent years, the applications of TiO_2 nanoparticles in the decomposition of various kinds of organic pollutants and the photoelectrochemical conversion of solar energy have been extensively studied because of its strong oxidizing ability, high photostability, nontoxicity, low cost as well as its chemical and biological inertness [1-8]. However, wide use of TiO_2 photocatalytic technology has been restricted mainly by the low visible light utilization efficiency due to its wide band gap (3.2eV) [9-12]. It has been reported that various factors influence the photocatalytic activity of TiO_2, such as phase structure, crystallite size [13,14], lattice defects, specific surface area, surface hydroxyls [15]. So far, a number of methods including chemical precipitation, hydrothermal method, magnetron sputtering technique and sol-gel method [16,17] have been applied for preparing TiO_2 nanoparticles. The sol-gel process has been proven to be suitable to prepare homogeneous pure and doped titania powders with the properties above [18].

Modification of TiO_2 with transition (either noble or lanthanide) metals were presented as a successful and cost effective alternative to increase its efficiency as photocatalyst, since transition metal ions modified its microstructures and electronic structures [19-21]. Zn-doped TiO_2 has been proven to be an effective mechanism for photocatalysis because of tie corrosion, hardness, semiconductor and magnetic preoperties, good transparency, and electron mobility. Moreover, the separation rate of the photoinduced charge was shown to be increased when zinc ions were used because of the difference in the energy band positions. Lu et al. prepared an efficient photocatalyst Zn^{2+}–TiO_2 by the sol–gel method [22]. Experiment indicated that Zn doping reduced the crystallite size of TiO_2 and the agglomeration of TiO_2 powder, thus displayed higher photocatalytic activity and regeneration ability than TiO_2.

In this paper, TiO_2 nanoparticles were synthesized by sol-gel method with two different procedures. On the basis of the method above, Zn-doped TiO_2 were obtained. At the same time, the effects of calcination temperatures and Zn doping amounts were discussed. The phenol degradation experiments of samples were conducted under three kinds of lights. The structure characteristics characterization and analysis of as-prepared samples were studied by XRD, BET, XPS, UV-vis DRS and TEM.

2. Experimental

2.1. Materials

Tetrabutyl titanate ($Ti(OC_4H_9)_4$) was obtained from Tianjin Guangfu Institute of Fine Chemicals. Zinc chloride ($ZnCl_2$) was obtained from Tianjin Guangfu Technology Development Co., Ltd. Absolute ethyl alcohol (CH_3CH_2OH) and Acetic acid (CH_3COOH) were obtained from Beijing Chemical Works. All the reagents were of analytical grade and were used without further purification. The water used was distilled.

2.2. Photocatalysts preparation

In sol-gel processes, TiO_2 is usually prepared by the reactions of hydrolysis and polycondensation of titanium alkoxides.The reactions can be described as follows [17]:

1. Hydrolysis

$$Ti(OC_4H_9)_4+H_2O\rightarrow Ti(OC_4H_9)_3OH+C_4H_9OH \quad (1)$$
$$Ti(OC_4H_9)_3OH+H_2O\rightarrow Ti(OC_4H_9)_2(OH)_2+C_4H_9OH \quad (2)$$
$$Ti(OC_4H_9)_2(OH)_2+H_2O\rightarrow Ti(OC_4H_9)(OH)_3+C_4H_9OH \quad (3)$$
$$Ti(OC_4H_9)(OH)_3+H_2O\rightarrow Ti(OH)_4+C_4H_9OH \quad (4)$$

2. Polycondensation

$$Ti(OH)_4+Ti(OC_4H_9)_4\rightarrow 2TiO_2+4C_4H_9OH \quad (5)$$
$$2Ti(OH)_4\rightarrow 2TiO_2+2H_2O \quad (6)$$

TiO_2 nanoparticles were prepared by sol-gel method with two different procedures. TiO_2 with procedure A was prepared as follows: solution A was consisted of CH_3CH_2OH, CH_3COOH and H_2O. Then solution A was added drop by drop to solution B consisting of $Ti(OC_4H_9)_4$ and CH_3CH_2OH under continuous stirring. The obtained homogeneous solution was magnetically stirred continuously for 1h and aged at room temperature for 24h to form a gel. The gel was washed with H_2O for three times and then dried in an oven at 120℃ until a dry gel was obtained. The dry gel was calcined in a muffle furnace at 450, 550 and 650℃. TiO_2 with procedure B was prepared as follows: solution C was consisted of CH_3CH_2OH and H_2O. Then solution C was added drop by drop to solution D consisting of $Ti(OC_4H_9)_4$, CH_3COOH and CH_3CH_2OH under continuous stirring. The following steps were the same as procedure A. The dry gel was calcined in a muffle furnace at 350, 450, 550, 650 and 750℃. Zn-doped TiO_2 was synthesized as follows: $ZnCl_2$ solution was added to solution C and the other steps were the same as the synthesis of undoped TiO_2 of procedure B. Zn-doped TiO_2 was calcined at 450℃. The undoped TiO_2 were donated as T-A/B-X (X presented temperature, respectively). The molar ratios of Zn in the Zn-doped TiO_2 were 1%, 2%, 3%, 4% and 5% and defined as ZTB-N (N presented the molar ratio of Zn/Ti).

2.3. Characterization

The crystal structures of the photocatalysts were examined with a powder X-ray diffractometer (XRD) (BRUKER D8 ADVANCE, Cu Kα, λ=1.54056 Å). The Brunauer−Emmett−Teller (BET) surface area and Barrett−Joyner−Halenda (BJH) pore size distribution measurements were carried out with ASAP 2020 Micromeritics USA. X-ray photoelectron spectra (XPS) analysis was conducted through an X-ray photoelectron spectrometer (Thermo ESCALAB 250) with an Al Ka (1,486.7eV) X-ray source. UV-visible reflectance spectra (UV-vis) for the samples were collected on a UV-visible spectrometer (UV-2550, SHIMADZU Corporation) to reveal their light activity (absorbance). Transmission electron microscopy (TEM) was recorded on a FECNAI F20 microscope. The concentration of phenol was measured by 4-aminoantipyrine spectrophotometric method on a UNICO 2100 visible spectrophotometer at 510 nm. The light intensity was tested by a digital luminance meter (TES-1332A, TES Electrical Electronic Corp.).

2.4 Photocatalytic activity experiment

The photocatalytic activity experiment of prepared nanoparticles was conducted in a quartz glass (Φ7×8cm). In each experiment, 0.3g photocatalyst was added to 300mL of 10mg·L^{-1} phenol solution under an oxygen flow and stirred for 30min to reach equilibrium absorption. Three kinds of light sources were used: 500-W xenon lamp, 500-W xenon lamp with a 430nm cutoff glass optical filter and natural solar light outdoor (Sep. 18, 2013; N43.88W, E125.32W). Every 1h, filtered solution was used for the UV-Vis absorption test.

3. Results and discussion

3.1X-ray diffraction

It can be seen from Fig. 1 that calcination temperatures had great effects on catalyst surface and structural features [23]. When TiO_2 powder was calcined at 350-750℃, the transformations from amorphous to anatase and rutile phase occurred. With calcination temperature increasing, anatase TiO_2 decreased and rutile TiO_2 increased ceaselessly (Table 1).

Obviously, the phase transformation from anatase to rutile occured between 550℃ and 650℃. And at 750℃, the crystal phase structure completely turned into rutile phase. The height of the peaks of ZTB-4 sample was shorter than that of T-B-450 sample. It revealed that the Zn doping could inhibit the transformation from anatase to rutile at elevated temperature. The average crystallite size of photocatalysts is shown in Table 2, calculated according to the Debye–Scherrer equation:

$$D=K\lambda / \beta \cos\theta$$

where D is the average crystallite size in angstroms, K is a dimensionless constant (0.89 here), λ is the wavelength of the X-ray radiation (Cu Kα =0.15406 nm), β is the full width at half-maximum (FWHM) of the diffraction peak and θ is the diffraction angle [24].

Table 1. The percentage of anatase and rutile of T-B with different calcination temperatures.

Sample	T-B-350	T-B-450	T-B-550	T-B-650	T-B-750
Percentage(anatase,rutile)(%)	—	100.0, 0.0	100.0, 0.0	46.2, 53.8	7.0, 93.0

Table 2. Average crystallite size of photocatalysts.

Sample	T-B-350	T-A-450	T-B-450	ZTB-4	T-B-550	T-B-650	T-B-750
Crystallite size(nm)	5.7	10.2	9.4	9.2	15.3	25.6	20.5

Table 3. Surface area, pore volume and pore size of T-B-450 and ZTB-4.

Smaple	Surface area(m^2/g)	Pore volume (cm^3/g)	Pore size (BJH)(nm)
T-B-450	83.37	0.09	4.28
ZTB-4	87.40	0.18	8.23

Table 4. The light intensity of solar light.

Time(h)	0	1	2	3	4	5	6	7	8
Intensity(lux)	35000	46500	65000	78000	83000	71000	64500	55400	45500

It was clearly observed from the XRD patterns that with the increase of calcination temperature, the diffraction peaks became sharper and stronger, which suggested that the crystalline quality of the nanoparticles was improved. And the crystallite size increased with the increasing temperature, which might be caused by particle agglomeration under high temperatures.

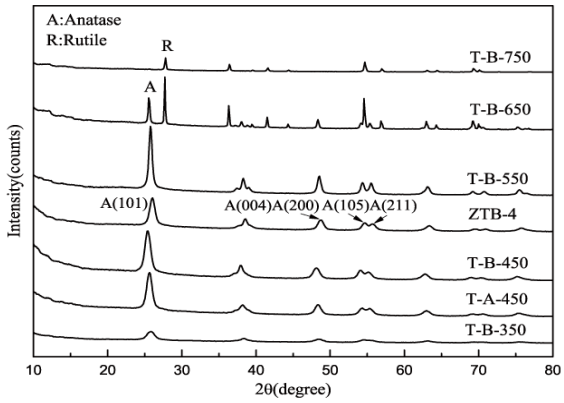

Fig. 1. XRD patterns of photocatalysts.

Generally, the anatase phase TiO_2 was reported with high photocatalytic activity [25]. It can be noted that T-B-450 sample has significant diffraction peaks (25.3°, 37.9°, 48.1°, 54.0°, 55.1°, 62.7°, 69.0°) presenting the characteristic of anatase phase [26]. Due to the low Zn content, the doping Zn atoms caused a slight shift in peak position of TiO_2, but the possible impurities such as zinc oxide were not detected [5]. It can be seen that the crystallite size of T-B-450 and ZTB-4 were 9.4nm and 9.2 nm. The results indicated that Zn doping did not much affect the crystallite size of TiO_2 nanoparticles [5].

3.2 BET analysis

The N_2 adsorption−desorption isotherm of T-B-450 and ZTB-4 indicated a specific surface area of 83.37m^2/g and 87.40m^2/g by BET analysis (Table 3) while the crystallite size of T-B-450 and ZTB-4 was 9.4nm and 9.2nm (Table 2). It suggested that the samples with smaller crystallite size had larger surface area, which was in aggreement with previous studies. The photocatalytic activity of ZTB-4 was higher than T-B-450, which could be attributed to the large surface area of ZTB-4. The pore

size of samples indicated that they were mesoporous nanoparticles.

3.3 XPS spectrum

It could be seen from Fig. 2a that there was a shift in the peak positions of Ti2p which could be explained in terms of the electron destiny around Ti depending upon different electronegativities of Ti and Zn ions. Two peaks at 458.5 and 464.2eV in T-B-450 sample corresponded to the Ti $2p_{3/2}$ and Ti $2p_{1/2}$ states, indicating that Ti is 4+ valence. However, the Ti $2p_{3/2}$ and Ti $2p_{1/2}$ peaks were at 459.05eV and 464.75eV in the ZTB-4 sample which indicated that there were at least two kinds of chemical states. This might attribute to the surface species such as Ti–OH and Ti–O–O resulting from the chemisorbed water (OH) [27]. The formation of Ti with lower valence could be attributed to the existence of lots of oxygen vacancies in the nanoparticles after Zn doping [5]. O1s peak at 529.8eV came from O-Ti-O linkages in T-B-450, while the ZTB-4 sample shifted to 530.35eV. The increase of the binding energy indicated that electronic interactions changed owing to the substitution of Ti by Zn [28].

The XPS results of Zn 2p state in ZTB-4 is presented in Fig. 2b where two peaks at about 1022.1 and 1045.0eV were assigned to the $2p_{3/2}$ and $2p_{1/2}$ electronic states of Zn(II), respectively. It indicated that Zn existed as the 2+ oxidation state in the system [29]. Therefore, it could be confirmed that Zn ions existed mainly in the form of ZnO clusters and dispersed on TiO_2 crystallite surfaces [28].

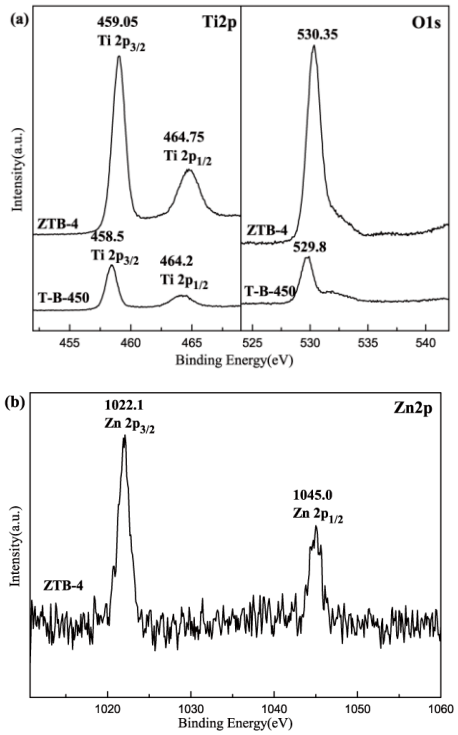

Fig. 2. X-ray photoelectron spectra of T-B-450 and ZTB-4: (a) Ti2p and O1s spectra; (b) Zn2p spectra.

3.4UV-Vis DRS analysis

The absorption spectra of the samples showed an obvious increase in the visible light region compared with P25. It showed absorption edge around 443nm for both T-A-450 and T-B-450, respectively. It could be observed a large redshift comparing to p25. The absorption decreased with calcination temperatures rising.

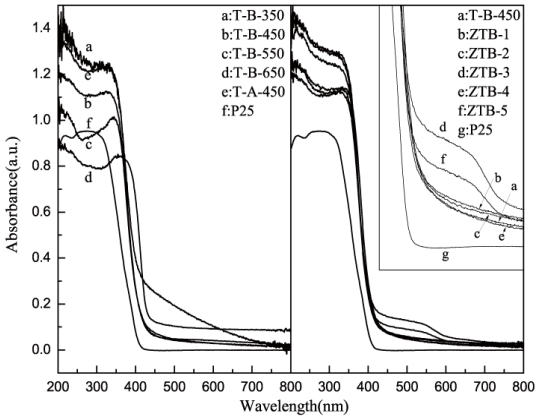

Fig. 3. UV-vis absorption of photocatalysts.

The oneset of the absorption spectrum of P25 appearing at about 387nm matched well with the intrinsic band-gap of anatase (3.2eV). It was obviously that there was a significant shift to the higher wavelength for all the Zn-doped samples compared to P25 and the absorption were stronger in the range of wavelengths from 400 to 600nm. This illustrated that Zn doping decreased the band gap energy and resulted in the red shift [30]. The corresponding band gap energy of P25, T-B-450 and ZTB-4 photocatalysts were 3.15, 3.04 and 2.97eV, based on

$$Eg = 1240 / \lambda$$

where Eg(eV) is the band gap and λ(nm) is the wavelength of the absorption edge in the spectrum.

3.5 TEM analysis

The microstructures of T-A-450, T-B-450 and ZTB-4 are presented in Fig. 4. All the TEM pictures showed the ordered porous structure of channels which indicated all the samples were consisted of highly crystalline and compact nanoparticles. The SAED pattern (insets of Fig. 4) displayed obvious rings, indicative of a polycrystalline structure.

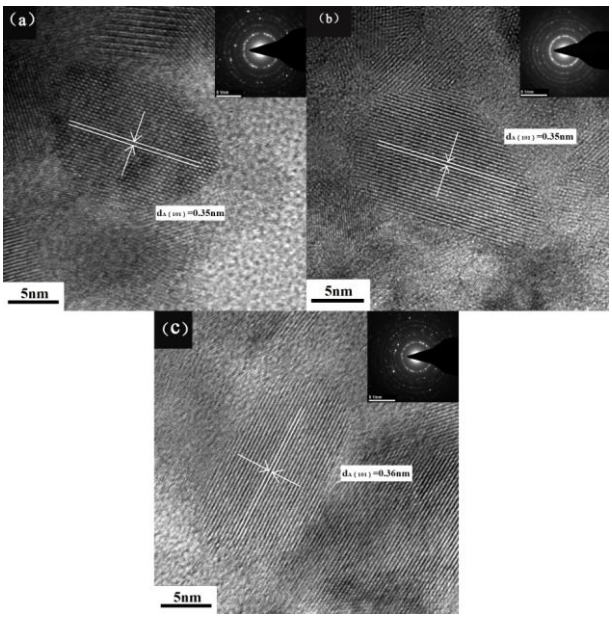

Fig. 4. TEM images of photocatalysts: (a) T-A-450; (b) T-B-450; (c) ZTB-4. The insets show the corresponding SAED pattern.

It indicated that in the T-A-450, T-B-450 and ZTB-4, there existed a lattice spacing (0.35, 0.35 and 0.36 nm) which was anatase TiO_2. However, anatase was not always morphologically the same, and the particles with anatase phase might not have the same photocatalytic properties.

3.6Photocatalytic activity

Four kinds of factors are discussed in Fig. 5: procedures of synthetizing TiO_2, calcination temperatures, Zn doping amounts and the influence of the lights. It showed that at the same calcination temperatures (450℃, 550℃ and 650℃), T-B samples all exhibited better photocatalytic activity than T-A samples. The residual rate of phenol using T-A-450 and T-B-450 was 27.6% and 2.2%, which could be attributed to the large surface area and small crystallite size of T-B-450 (Table 2, 3). In addition, adding acetic acid directly to the $Ti(OC_4H_9)_4$ solution (procedure B) can not only accelerate the hydrolysis rate of titanium alkoxides but also slow the polymerization reaction rate of titanium alkoxides [31].

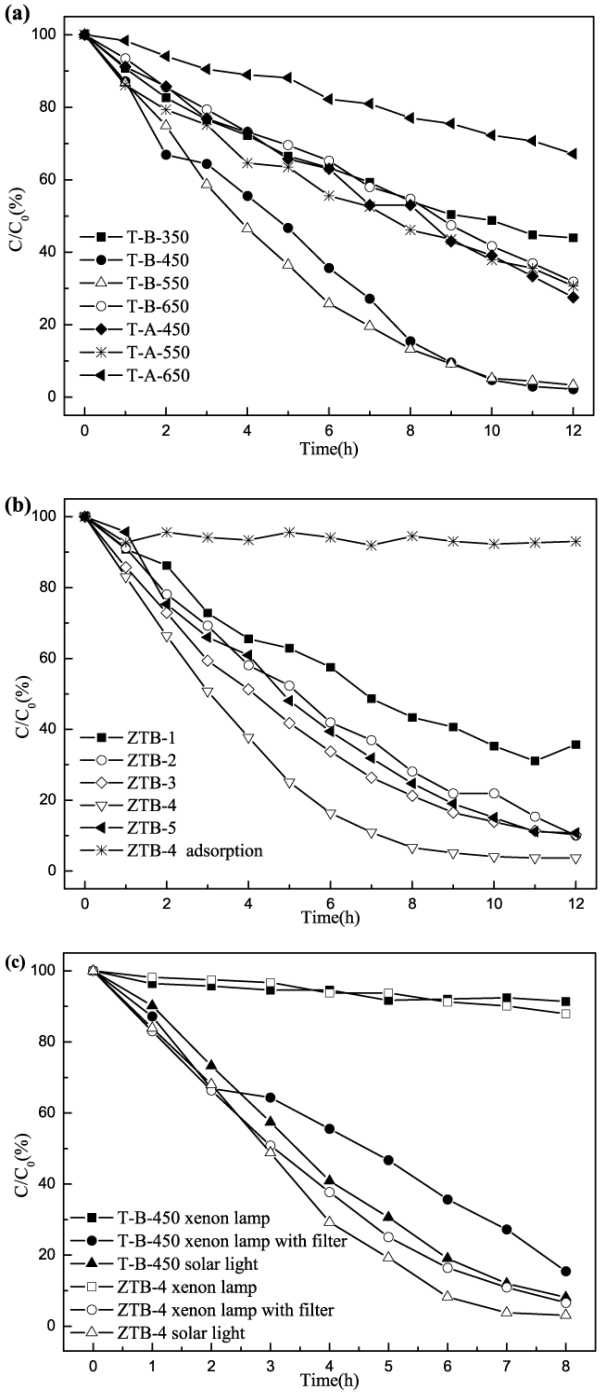

Fig. 5. Photocatalytic activity of photocatalysts (phenol 10 mg/L; photocatalyst 1.0 g/L): (a) T-A and T-B with different calcination temperatures; (b) Photocatalytic activity of T-B with different Zn doping amounts and adsorption property of ZTB-4; (c) T-B-450 and ZTB-4 under different light source (xenon lamp 7000 lux, xenon lamp with a 430nm cutoff glass filter 2100lux and solar light, Table 4).

Calcination temperatures had a remarkable influence on the structural properties of photocatalyst and resulted

in great effects on degradation efficiency [32]. Among the catalysts, the photocatalytic activity increased with the increase of calcination temperatures from 350 to 450℃. At 450℃, the catalyst reached the highest activity. This should mainly result from small nano-sized particle and the anatase phase which was in agreement with the previous study [25]. With calcination temperatures further increasing, crystallite size as well as rutile content of catalyst increased (Fig. 1 and Table 3) and its photocatalytic activity decreased. Meanwhile, high temperature could bring about particle agglomeration and decrease the surface area of photocatalysts, which also affect the efficiency. The results showed that the phase composition, anatase content and crystallite size of photocatalysts played an important role in high photocatalytic activity.

On the basis of doping theory [33], an optimal dopant concentration was critical for the catalysts. Among T-B with different Zn doping amounts, ZTB-4 was most efficient. Because by increasing the Zn amount up to 4 mol%, the lifetime of the charge carriers increased, which led more hydroxide ions to attract on the nanoparticles surface and prevented the photoinduced electron-hole pair recombination. However, more doping would lead to the formation of excessive surface oxygen vacancies, which would act as electron traps and retarded electron transfer process, thereby undermining the photocatalytic activities [5].

To compare the visible-light photocatalytic activity of samples, the phenol degradation experiments were conducted under three kinds of lights. The photocatalysts make use of light on different wave bands were not the same because of different band gap widths corresponding to different excitation wavelengths [34]. The adsorption reaction for ZTB-4 verified the amount of adsorption was very small compared with the photodegradation part (Fig. 5b). In the filter conditions, phenol concentration changed very slightly. It indicated that the absorption edge of Zn-doped TiO_2 had a slight redshift, but it was still difficult to utilize the long-wavelength light (>> 440 nm) efficiently. The degradation effect of all samples were excellent under solar light which suggested the samples can make full use of solar light. These results indicated that Zn doping enhanced the photocatalytic activity and improved the utilization of solar light.

4. Conclusions

Undoped and Zn-doped TiO_2 nanaoparticles were successfully synthesized by sol-gel method with two different procedures. XRD results showed that with calcination temperatures increasing, anatase TiO_2 decreased and rutile TiO_2 increased and the crystallite size increased. Zn doping could inhibit the transformation from anatase to rutile. Zn existed as the 2+ oxidation state in the Zn-doped TiO_2. UV-vis adsorption indicated the optical absorption edges of Zn-doped samples shifted to longer wavelength regions. It was found that the photocatalytic activity of TiO_2 -B was much higher than TiO_2 -A. The optimal calcination temperature and Zn doping amount was 450℃ and 4% for Zn-doped TiO_2. Zn doping enhanced the photocatalytic activity and improved the utilization of solar light.

Acknowledgements

This work was supported by the National Natural Science Foundation of China (No. 51308252), Jilin Province Science and Technology Development Plans (No.20130101091JC) and the analysis and testing foundation of Jilin University and Changchun Technology Innovation Fund (No. 2009086).

References

[1] R. Vicente, J. Soler, A. Arques, A. M. Amat, Z. Frontistis, N. Xekoukoulotakis, D. Mantzavinos, J Chem Technol Biotechnol. **89**, 1259 (2014).
[2] Y.-P. Tsai, R.-A. Doong, J.-C. Yang, Y.-J. Wu, J Chem Technol Biotechnol. **86**, 949 (2011).
[3] T.-L. Su, Y.-L. Kuo, T.-J. Wu, F.-C. Kung, J Chem Technol Biotechnol. **87**, 160 (2012).
[4] L. G. Devi, B.N. Murthy, S. G. Kumar, Mate Sci Eng B. **166**, 1 (2010).
[5] Y. Zhao, C. Li, X. Liu, F. Gu, H. Du, L. Shi, Appl Catal B Environ. **79**, 208 (2008).
[6] M. Bettinelli, V. Dallacasa, D. Falcomer, P. Fornasiero, V. Gombac, T. Montini, L. Romano, A. Speghini, J Hazard Mater. **146**, 529 (2007).
[7] S. Wang, Y. Huang, Optoelectron. Adv. Mater.-Rapid Comm. **8**, 770 (2014).
[8] C. Jiao, W-Q. Huang, G-F. Huang, Z-D. Su, M-G. Xia, Z-M. Yang, Z. Wan, Q-L. Zhang, Optoelectron. Adv. Mater.-Rapid Comm. **8**, 647 (2014).
[9] K. Li, Y. He, Y. Xu, Y. Wang, J. Jia, Environ Sci Technol. **45**, 7401 (2011).
[10] Y. Liu, J. He, Y. Sun, J. Hu, C. Li, G. Xue, S. Ognier, J Chem Technol Biotechnol. **88**, 1815 (2013).
[11] C. Obreci, M. Totu, S. K. Tanczos, E. Vasile, A. Dinu, A. C. Nechifor, Optoelectron. Adv. Mater.-Rapid Comm. **7**, 822 (2013).
[12] J-G. Huang, J-C. Shi, G. Liu, X-D. Hu, L-L. Dong, X-G. Zhao, X-J. Liu, Optoelectron. Adv. Mater.-Rapid Comm. **8**, 679 (2014).
[13] K. Tanaka, M. F. Capule, T. Hisanaga, Chem Phys Lett. **187**, 73 (1991).
[14] Z. Zhang, C.-C. Wang, R. Zakaria, J. Y. Ying, J Phys Chem B. **102**, 10871 (1998).
[15] M. Seabra, I. Salvado, J. Labrincha, Ceram Int. **37**, 3317 (2011).
[16] A. Agafonov, A. Vinogradov, J Sol-Gel Sci Technol. **49**, 180 (2009).

[17] Z. J. Chen, G. L. Zhao, H. Li, J. J. Zhang, B. Song, G. R. Han, Chin. J. Inorg. Chem. **26**, 860 (2010).
[18] C. Chen, Z. Wang, S. Ruan, B. Zou, M. Zhao, F. Wu, Dyes and Pigments. **77**, 204 (2008).
[19] E. Arpac, F. Sayılkan, M. Asiltürk, P. Tatar, N. Kiraz, H. Sayılkan, J Hazard Mater. **140**, 69 (2007).
[20] R. Marotta, I. Di Somma, D. Spasiano, R. Andreozzi, V. Caprio, J Chem Technol Biotechnol. **88**, 864 (2013).
[21] X-W. He, C-Z. Liu, X-H. Yu, D-W. Meng, J-F. Chen, C. Lu, X-L, Wu, Optoelectron. Adv. Mater.-Rapid Comm. **8**, 672 (2014).
[22] X. Lu, J. Jiang, K. Sun, D. Cui, Appl Surf Sci. **258**, 1656 (2011).
[23] J. Yu, L. Zhang, B. Cheng, Y. Su, J Phys Chem C. **111**, 10582 (2007).
[24] M. Yan, F. Chen, J. Zhang, M. Anpo, J Phys Chem B. **109**, 8673 (2005).
[25] A. Fujishima, T. N. Rao, D. A. Tryk, J Photochem and Photobiol C. **1**, 1 (2000).
[26] C. Xu, R. Killmeyer, M. L. Gray, S. U. Khan, Appl Catal B Environ. **64**, 312 (2006).
[27] J.-G. Yu, H.-G. Yu, B. Cheng, X.-J. Zhao, J.C. Yu, W.-K. Ho, J Phys Chem B. **107**, 13871 (2003).
[28] Q. Liu, Y. Zhou, Y. Duan, M. Wang, Y. Lin, Electrochim Acta. **95**, 48 (2013).
[29] H. R. Zhang, Y. Liang, X. D. Wu, H. W. Zheng, Mater. Res. Bull. **47**, 2188 (2012).
[30] Y.-Z. Wang, X.-X. Xue, H. Yang, Chin. J. Inorg. Chem. 28 (2013).
[31] D-H. Yin, D-Y. Deng, E-W. Chen, D-L. Yin, Ind Catal. **12**, 1 (2004).
[32] J-G. Huang, M-Y. Zheng, S. Pang, L-G. Liu, L-L. Dong, X-J. Liu, Reac Kinet Mech Cat. **113**, 281 (2014).
[33] W. Choi, A. Termin, M.R. Hoffmann, J Phys Chem. **98**, 13669 (1994).
[34] J.-G. Huang, X.-G. Zhao, M.-Y. Zheng, S. Li, Y. Wang, X.-J. Liu, Water Sci Technol. **68**, 934 (2013).

*Corresponding author: donglili104@163.com